

Cost-effective Framework for Rapid Underwater Mapping with Digital Camera and Color Correction Method

Anjin Chang*, Jinha Jung**, Dugan Um***, Junho Yeom****, and Frederick Hanselmann*****

Received October 10, 2018/Accepted November 21, 2018/Published Online February 26, 2019

Abstract

Geo-referenced mapping in an aquatic environment is challenging because it is hard to measure the location of objects and images underwater. In this paper, we propose the method and share the results: cost-effective framework to generate 2D and 3D underwater maps with digital imagery and a Structure from Motion (SfM) algorithm. The proposed method consists of data acquisition, image processing, and color correction. 292 and 437 images were acquired from each study site located in Spring Lake in San Marcos, Texas, U.S.A. Agisoft Photoscan Pro software was used to generate 3D point cloud data and orthomosaic images after feature matching and image alignment from geo-tagged imagery. The mosaic images with high resolution (< 0.2 cm per pixel) were generated with 2D underwater images. After color correction, the red reduction effect was recovered, and the bluer color was removed. The 3D underwater map was generated directly from 3D dense point clouds including geo-coordinates and RGB color information. As a result, the Very High Resolution (VHR) 2D and 3D maps were generated and the topographic surface of underwater structures was obtained in great detail. Although the RMSE were about 1 m, the proposed method provided more detailed surface of underwater features.

Keywords: *underwater, Structure from Motion (SfM), 3D mapping, bathymetry, underwater color correction*

1. Introduction

Understanding the underwater environment and generating an underwater map have received great attention in the fields of survey, hydrology, ecology, and archaeology (Roman *et al.*, 2011; Figueira *et al.*, 2015; VanMiddlesworth *et al.*, 2015; Balletti *et al.*, 2016; Atallah and Probert Smith, 2003). Underwater environments can be harsh and demanding in regard to the collection of photographic data and locational data due to limitations such as poor light condition, limited operation time, lack of visibility, strong currents, temperature, and other technical difficulties. Due to such difficulties in collecting geo-referenced three-dimensional (3D) underwater data, many researchers have utilized various remote sensing techniques. For example, sonar sensors, bathymetric LiDAR (Light Detection And Ranging), and photogrammetry have been used for deep water oftentimes controlled via platforms such as Autonomous Underwater Vehicles (AUV's) or Remotely Operated Vehicles (ROV's). While deep-

water imagery has advanced more rapidly, bathymetric LiDAR (Light Detection and Ranging) and photogrammetry also have important applications within a shallow water environment (< 40 m).

Sonar systems detect backscatter reflection from underwater objects to generate a bathymetric map (Atallah and Probert Smith, 2003). Geo-location is determined using GPS signal to track the sonar sensor's position, while the sonar data was recorded separately (Hasan *et al.*, 2012; Hooge *et al.*, 2016). Lu and Cho (2010) proposed a water-depth correction algorithm for seagrass mapping using airborne hyperspectral data. VanMiddlesworth *et al.* (2015) created an underwater 3D map by using profiling sonar acquired from AUV's. The locations were relatively estimated by the Simultaneous Localization And Mapping (SLAM) and by the Iterative Closet Point (ICP) algorithm. A 3D model of the seafloor is then generated by the acquired stereo imagery and SLAM-based vehicle poses (Johnson-Roberson *et al.*, 2010).

Detailed bathymetric data can also be generated from the

*Member, Research Assistant Professor, School of Engineering and Computing Sciences, Texas A&M University-Corpus Christi, TX 78412, USA (E-mail: anjin.chang@tamucc.edu)

**Assistant Professor, School of Engineering and Computing Sciences, Texas A&M University-Corpus Christi, TX 78412, USA (Corresponding Author, E-mail: jinha.jung@tamucc.edu)

***Associate Professor, School of Engineering and Computing Sciences, Texas A&M University-Corpus Christi, TX 78412, USA (E-mail: dugan.um@tamucc.edu)

****Member, Research Assistant Professor, Research Institute for Automotive Diagnosis Technology of Multi-scale Organic and Inorganic Structure, Kyungpook National University, Sangju 37224, Korea (E-mail: salt2525@knu.ac.kr)

*****Director, Underwater Archaeology and Underwater Exploration, Dept. of Marine Ecosystems and Society, University of Miami, FL 33149, USA (E-mail: fhanselmann@rsmas.miami.edu)

LiDAR system and could provide a practical approach for relating biotic and geophysical factors across large extents of shallow water, such as detecting seagrass distribution, classifying algae, and discriminating coral from non-coral habitats (Wang and Philpot, 2007; Vierline *et al.*, 2008; Walker *et al.*, 2008; Zavalas *et al.*, 2014). Although sonar and airborne LiDAR cover across the wide range of area and the cost for data acquisition has decreased rapidly, the piloted airborne platform remains cost intensive and boat-towed sensors are time intensive. Additionally, both platforms require an operator. In addition, integration of sensor data and the GPS signal is an intriguing job. Furthermore, underwater texture and weather conditions are critical issues for data acquisition. Multi-beam sonar is the one of main technologies to generate a bathymetric map and to record backscatter signal. Although multi-beam sonar data would be useful to analyze the seafloor and to map habitats and coral reefs, it provides only elevation and intensity of signal without including color information (Roberts *et al.*, 2005; Brown and Blondel, 2009).

With the development of Structure from Motion (SfM) technology, which is a photogrammetric technique for the common digital camera, the issues related to the cost and limitations of traditional remote sensing techniques have allowed for the generation of 3D models for topographic and underwater mapping, especially in shallow water (Fonstad *et al.*, 2013; Dietrich, 2017). The 3D model of any underwater structure can be created from multiple images by SfM algorithm without additional information such as Interior Orientation (IO), Exterior Orientation (EO), and Ground Control Points (GCP) (Figueira *et al.*, 2015; González-Rivero *et al.*, 2016). In general, GCPs of Areas Of Interest (AOI) and EO, meaning camera locations and orientations, of each image have been used to generate 3D point clouds or mesh from multiple images, from which geo-referenced and ortho-rectified mosaic images are created (Fonstad *et al.*, 2013; Wolf and DeWitte, 2000). However, it is very difficult to select GCPs and collect their geo-coordinates with GPS or total station underwater. Few researchers tried to install GCPs and measure the underwater coordinates with GPS attached long poles. It is labor-intensive, expensive and time-consuming process (Balletti *et al.*, 2016). Although many studies have used the SfM algorithm to generate 3D models for underwater environments, the target is shallow water or the produced models are not as precisely in sync with their associated geo-coordinates. Google teamed up with the Catlin Seaview Survey to record underwater panoramic views for monitoring coral reefs and offers Street View Oceans (Google Street View). González-Rivero *et al.* (2016) collected underwater images over coral reefs taken by a diver with a digital camera mounted on a semi-auto system for ecological data measurements. 3D models of individual coral colonies and patches of reef area were generated in order to evaluate the precision and accuracy of geometry and structural complexity metrics by repeated modelling and comparison with laser reference models (Figueira *et al.*, 2015; Ferrari, 2016). Dietrich (2017) extracted shallow stream bathymetry from multi-view stereo photogrammetry by correcting for refraction.

Due to ever-changing underwater lighting conditions, the color of the images must be normalized. The red spectrum attenuates faster underwater than blue or green spectrums because of its longer wave length. A color correction algorithm is adopted and used to correct the color of images for more realistic photographing by enhancing the attenuated red band lost through absorption. In addition to color correction, the geo-referencing coordinates have to be adjusted as well for various applications such as mapping, navigation, underwater video recording, etc.

The focus of this study is the cost-effective framework for rapid 2D and 3D underwater mapping with SfM algorithm. Since time synchronization has to be assured, an underwater mapping apparatus was designed for geo-tagging between images and GPS location. A method by Ruderman's opponent color space $\alpha\beta$ was adopted for color correction in this study (Ruderman *et al.*, 1998; Bianco *et al.*, 2015). While several studies already have used SfM algorithm for underwater mapping (Figueira *et al.*, 2015; Balletti *et al.*, 2016; Dietrich, 2017; Ferrari, 2016), we propose a practical method composed of a set of simple data acquisition methods, including geo-tagging, image processing, and color correction in order to provide ortho-rectified mosaic images and 3D point cloud from underwater camera images.

2. Study Area and Materials

The test site was Spring Lake located in San Marcos, Texas, U.S.A. The lake is managed by the Meadows Center for Water and the Environment at Texas State University (Fig. 1). Spring Lake has a unique freshwater ecosystem and transparent water, thus ideal for 3D mapping with the SfM technique. One of the greatest outflows from the Edwards Aquifer is the San Marcos Springs, located within Spring Lake. More than 200 springs burst forth from a mixture of high and low pressure artesian springs. The springs and the short 3.8-mile San Marcos River have been designated as critical habitat for several endangered species, including the Fountain Darter, the Texas Blind Salamander, the San Marcos Salamander, the San Marcos Gambusia, and Texas Wild Rice. It is also an important archaeological site with both terrestrial and underwater components, which has provided material cultural evidence of human activity for every period of Texas prehistory and a very interesting geomorphological depositional history (Hooge *et al.*, 2016). Inasmuch, Spring Lake was a perfect place to test this methodology.

As mentioned earlier, the precision geo-tagging between images and GPS signal is necessary for high quality underwater mapping. The Meadows Center has been operating glass-bottom boat tours for school groups and the generally public for years. Since Spring Lake is a nature preserve, we acquired the data on one of the boats using an RGB camera, a GPS logger, and a wooden pole (1.8 m). The camera with waterproof housing and GPS logger were installed at both ends of 1.8-meter-long pole (Fig. 2(a)). The camera was submerged in the water to take underwater images and the GPS coordinates were recorded



Fig. 1. Image of Spring Lake Captured from Google Maps (2016). Two red Circles Indicate the Location to Acquire Digital Imagery.

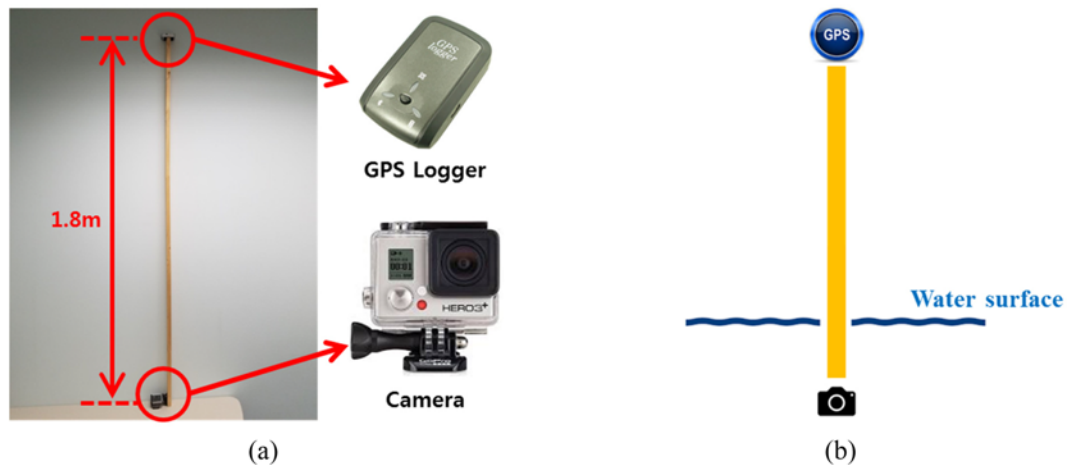


Fig. 2. Customized Underwater Imaging Equipment: (a) The Combined Equipment with RGB Camera, GPS Logger, and Pole, (b) The Concept Figure How to Take Underwater Images

simultaneously (Fig. 2(b)). Two areas, near-shore (site #1) and the middle of the lake (site #2) were selected as test sites (Fig. 1). Although over 1,500 images were taken through a route of the boat, 292 and 437 images were selected respectively, for 3D mapping of each site after removing low quality images including noisy, blurred, defocused, and unnecessary images. The overlap ratio between images was over 80% even though the data acquisition process was unstable due to inconsistent boat speed and manual carriage.

A “GoPro HERO 3+ Black edition”, manufactured by GoPro, Inc., CA, USA, was used to take RGB images and “i-Blue 747 Bluetooth GPS Data Logger” was used to record geo-location for image geo-referencing (G&V Global Tech Co., Ltd., Taipei City, Taiwan). The RGB camera has a 2.77 mm focal length and can take a picture up to 12 Megapixels (3,000 × 4,000 pixels) per half second. The GPS logger has 3 m accuracy and records the longitude, latitude, and elevation base on WGS 84

datum, 5 times per second. The GPS logger software was provided to show and export the time and coordinate of GPS signal. The laptop’s screen, which is synchronized with GPS logger, was taken by GoPro camera to calculate time-offset between GoPro camera and GPS logger prior to taking underwater images.

3. Method

3.1 Image Geo-tagging

Although the GPS signal included the exact time and was recorded 5 times per second, there is a time-offset between GPS time and image acquisition time since the GoPro camera has its own timer. Both GPS and camera timers should be synchronized for geo-tagging for optimal results. Since the GoPro camera can only display hours and minutes, the project laptop was used to calculate time-offset from when the GoPro camera was started

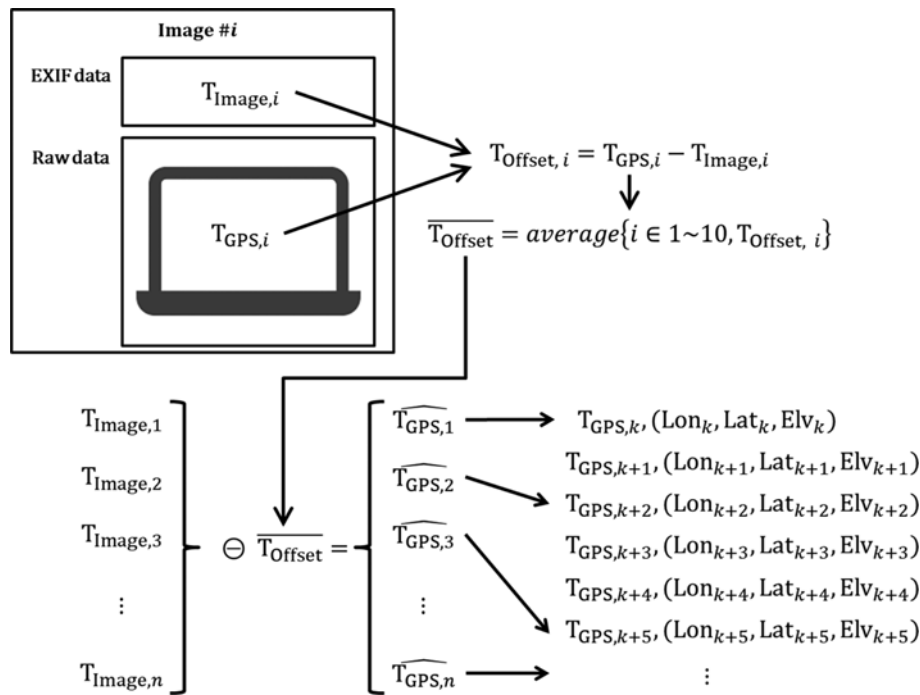


Fig. 3. The Concept of Geo-tagging by Calculating Time-offset between the GoPro Images and the GPS Signal

before submersion. The time-offset of a specific image can be calculated by subtracting image acquisition time in EXIF (header) from the GPS time on the laptop screen. Ten clear images taken before submerging the camera were selected and the average of the time-offset of those images was adopted as the overall time-offset (Fig. 3).

The acquisition time of all images was converted to estimated-GPS time ($\hat{T}_{GPS,i}$) using the time-offset for geo-tagging. Since the time interval of the GPS (0.2 s) and camera (0.5 s) was different, estimated-GPS time was matched up with the closest GPS time. The geo-coordinate (Longitude, Latitude, and Elevation) of each image was determined from the GPS logger data (Fig. 3). In addition, the length of the pole and geoid height were considered to determine the Above Sea Level (ASL) elevation. Finally, although there are a few concerns caused by absolute accuracy of the GPS logger, the different time interval of the camera, the GPS signal, and the variation of time-offset, the location of all images was approximated using time-based geo-tagging.

3.2 3D Point Cloud, Orthomosaic, and DSM Generation

In this study, the SfM algorithm was adopted to generate the 3D point cloud, the orthomosaic image, and the DSM (Digital Surface Model) from hundreds of underwater images with matching points. SfM is a photogrammetric range imaging technique to estimate 3D structures from 2D images. SfM performs a bundle adjustment among multiple images based on matching features in the overlapped area between images to estimate IO and EO. Although SfM could estimate IO and EO without the geometric information in advance, that information makes the processing faster if available. First of all, the features are

extracted from each image to be matched to their corresponding features in other images for aligning relative locations and the parameter of sensor (Lowe, 2004; Snavely *et al.*, 2008). After refining matched features, the 3D point cloud is generated by applying the multi-view stereo-matching algorithm to the images. Ortho-rectified mosaic images and the DSM are then generated from 3D point cloud and aligned images (Harwin *et al.*, 2015; Shao *et al.*, 2016).

Two data sets in the study area were processed using Photoscan Pro commercial software (AgiSoft LLC, St. Petersburg, Russia). Agisoft Lens was used to perform camera self-calibration (Balletti *et al.*, 2014). We entered the underwater images and image locations, arranged by geo-tagging steps to ensure alignment and to improve processing speed. Even with only partial EO information including longitude, latitude and elevation (X, Y, Z), Photoscan can estimate 6 parameters (X, Y, Z, ω , ϕ , κ) of each image and IO for further updates (Harwin *et al.*, 2015). Image alignment processing was conducted with image location and camera calibration parameters to calculate EO of all images, and then colored dense point cloud was built using aligned images and matching points between all images.

After generating 3D point clouds based on updated IO and EO, the point clouds, orthomosaic image, and DSM of two study sites were exported to display with Potree and Geotif. Potree is a web-based and open source viewer for large point cloud data (Schuetz, 2016). 3D point clouds from underwater images were converted to Potree's file system and then displayed in the web browser. The color correction method was applied to the orthomosaic images (see next section for more detail). Additionally, the DSM was compared with the referenced bathymetric maps to evaluate

the result of the proposed method.

3.3 Color Correction for Underwater Imagery

A novel method for color correction for underwater images was proposed by Bianco *et al.* (2015) and is based on gray-world and uniform illumination assumptions applied in the $\alpha\beta$ space Ruderman *et al.* (1998). The gray-world assumption is about achromatic, which means that the information in the average of each band (R, G, B) of a color image is a representative gray level. In addition, we assume that the light intensity is approximately constant over the whole image. The color space is composed of a luminance component l (achromatic) and two opponent color components and α and β (chromatic) as performed for color discrimination in the human color visual mechanism. Although there are several steps to convert a raw image (RGB) to the $\alpha\beta$ space, we describe the converting Eq. (1) with the transformations matrices Eqs. (2), (3), and (4) as follows:

$$l_{\alpha\beta,j}(m, n) = \mathbf{T}_{pca,ij} \cdot \log(\mathbf{T}_{lms,ij} \cdot \mathbf{T}_{xyz,ij} \cdot f_i(m, n)) \quad (1)$$

linear RGB \rightarrow XYZ space: $\mathbf{T}_{xyz,ij}$

$$= \begin{bmatrix} 0.5141 & 0.3239 & 0.1604 \\ 0.2351 & 0.6702 & 0.0641 \\ 0.0241 & 0.1228 & 0.8444 \end{bmatrix} \quad (2)$$

XYZ space \rightarrow LMS space: $\mathbf{T}_{lms,ij}$

$$= \begin{bmatrix} 0.3897 & 0.6890 & 0.0787 \\ -0.2298 & 1.1834 & 0.0464 \\ 0.0000 & 0.0000 & 0.0000 \end{bmatrix} \quad (3)$$

$\log(\text{LMS})$ space \rightarrow $l_{\alpha\beta}$ space: $\mathbf{T}_{pca,ij}$

$$= \begin{bmatrix} 1/\sqrt{3} & 0 & 0 \\ 0 & 1/\sqrt{6} & 0 \\ 0 & 0 & 1/\sqrt{2} \end{bmatrix} \begin{bmatrix} 1 & 1 & 1 \\ 1 & 1 & -2 \\ 1 & -1 & 0 \end{bmatrix} \quad (4)$$

where $i, j \in \{1, 2, 3\}$ are the matrix indices which is the number of bands for RGB and $\alpha\beta$, respectively, and (m, n) are the pixel coordinates (Reinhard *et al.*, 2001). The linear RGB images have to be imported as the input data, $f_i(m, n)$, for Eq. (1). The first element of $\alpha\beta$ vector is luminance (l) representing achromatic information and being proportional to intensity ($r + g + b$), while the second (α) and (β) third elements are chromatic and proportional to yellow-blue ($r + g - 2b$) and red-green ($r - g$) opponent bands (Bianco *et al.*, 2015).

Although the human visual system can perceive the true color of objects under various light source conditions, sensors are not able to distinguish between the color of the illuminance and the reflectance of the objects since they measure the incoming light from the objects. In digital images, the white balancing process has been adopted to avoid unrealistic color casts. Specifically, the red information was reduced and attenuated by its absorption the

deeper it travels in the water column. In order to correct color casts of underwater images, the chromatic information (α and β) have to be changed (Reinhard *et al.*, 2001). The value of the white color is (1, 1, 1) in linear RGB color, while α and β value is (0, 0). The median value of α and β was adopted to avoid the affection by extreme values for white balancing of the images as below:

$$l_{\alpha\beta,k}^*(m, n) = l_{\alpha\beta,k}(m, n) - \bar{l}_{\alpha\beta,k} \quad (5)$$

where $l_{\alpha\beta,k}^*(m, n)$ are the corrected vector, $l_{\alpha\beta,k}(m, n)$ is the converted vector of RGB image, and $\bar{l}_{\alpha\beta,k}$ is the median component of RGB (Bianco *et al.*, 2015). While β and ($k \in \{2, 3\}$) value were changed for color correction, the histogram equalization, which is the most popular contrast enhancement techniques, was applied to luminance channel (l) to improve the achromatic component. After color correction in the color space, the result has to be transferred back to RGB space by applying the inverse operations as below:

$$f_i^*(m, n) = \mathbf{T}_{xyz,ij}^{-1} \cdot \mathbf{T}_{lms,ij}^{-1} \cdot \exp(\mathbf{T}_{pca,ij}^{-1} \cdot l_{\alpha\beta,j}^*) \quad (6)$$

where $f_i^*(m, n)$ are the corrected linear RGB vector. Finally, the color corrected underwater orthomosaic image was generated. In this study, the orthomosaic images were converted to linear RGB so that the color correction algorithm could be applied, then the inverse transformations of color correction was applied to regenerate the color-corrected orthomosaic images in RGB color space.

4. Discussion

4.1 2D Underwater Mapping

Orthomosaic images of the test sites were exported from Photoscan software to display 2D underwater maps. The spatial resolution of the mosaic image for study sites #1 and #2 was calculated as 0.17 cm and 0.05 cm, respectively, because the depth of water of site #1 (about 4–4.3 m) is approximately three times deeper than site #2 (1.2–1.5 m) (Hooge *et al.*, 2016). Figs. 4(a) and 4(b) show the orthomosaic image of the study sites before color correction. The detailed underwater map was generated, while the satellite image in Google Earth at same location only indicates the surface image of the lake. Although distortion occurred around the boundary of the mosaic images due to non-overlapped area in raw images, the mosaic image had very-high spatial resolution and could indicate the detailed map despite moving objects such as fish and plants. Even the tiny objects such as weeds, plants, sand, fish, and branches could be distinguished in the constructed 3D model because of high quality underwater images (Fig. 4(c)). This implies that the result of the proposed method could be useful for underwater surveying, monitoring and navigation.

The results of color correction were evaluated by visual because the Spring Lake is the preserved natural area (Figs. 5(a) and 5(b)). The images before color correction looked greener and bluer because of red reduction from absorption in the water

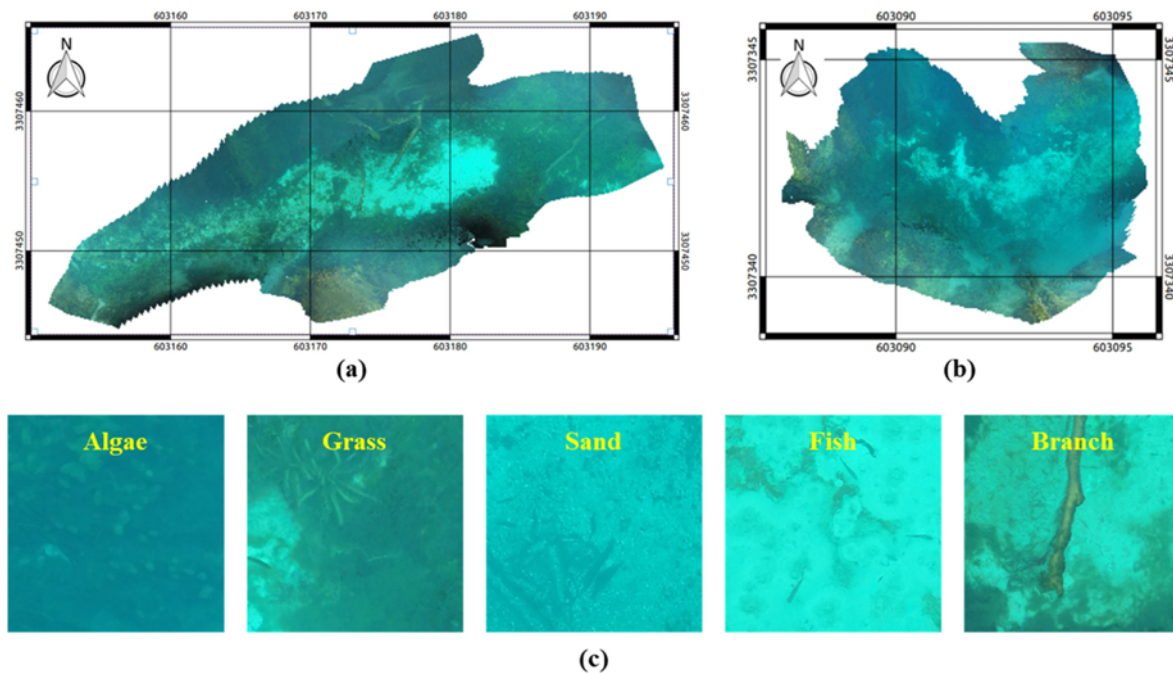


Fig. 4. The Orthomosaic Image for (a) Study Site #1, (b) site #2, and (c) the Magnified Images of Small Objects Underwater

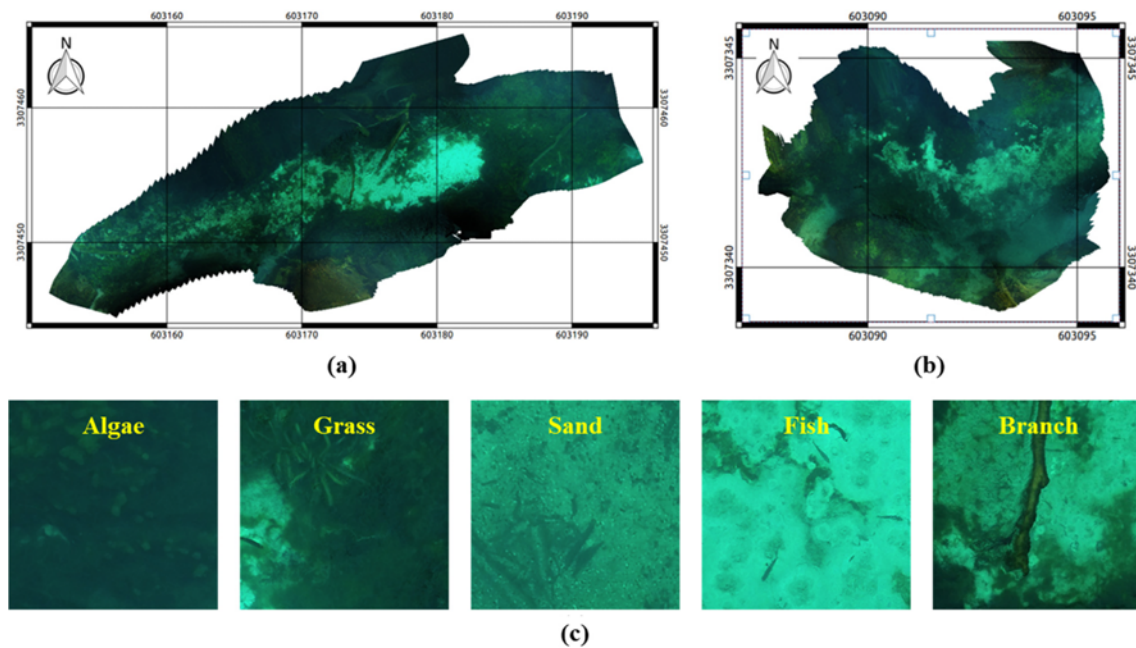


Fig. 5. The Orthomosaic Images of: (a) Study Site #1, (b) Site #2 after Color Correction, (c) The Magnified Images of Small Objects after Color Correction

column. We applied the color correction method of the $\lambda\beta$ space, described in Section 3.3, to the orthomosaic images to compensate red information. The red reduction effect was recovered, and the bluer effect was removed. The color of small objects was converted in general cases such as weeds (dark green and green), branches (brown) and sand (light yellow) (Fig. 5(c)). Although the corrected color was not perfectly the same as terrestrial conditions, the results were satisfactory with more realistic color

casts. Especially, underwater vegetation and sand are distinguishable visually.

4.2 3D Underwater Mapping

A 3D map is usually created from 3D model type data with mesh and texture, which is very time consuming and computationally intensive (Schobesberger and Patterson, 2008). In order to maximize efficiency, the 3D underwater map was

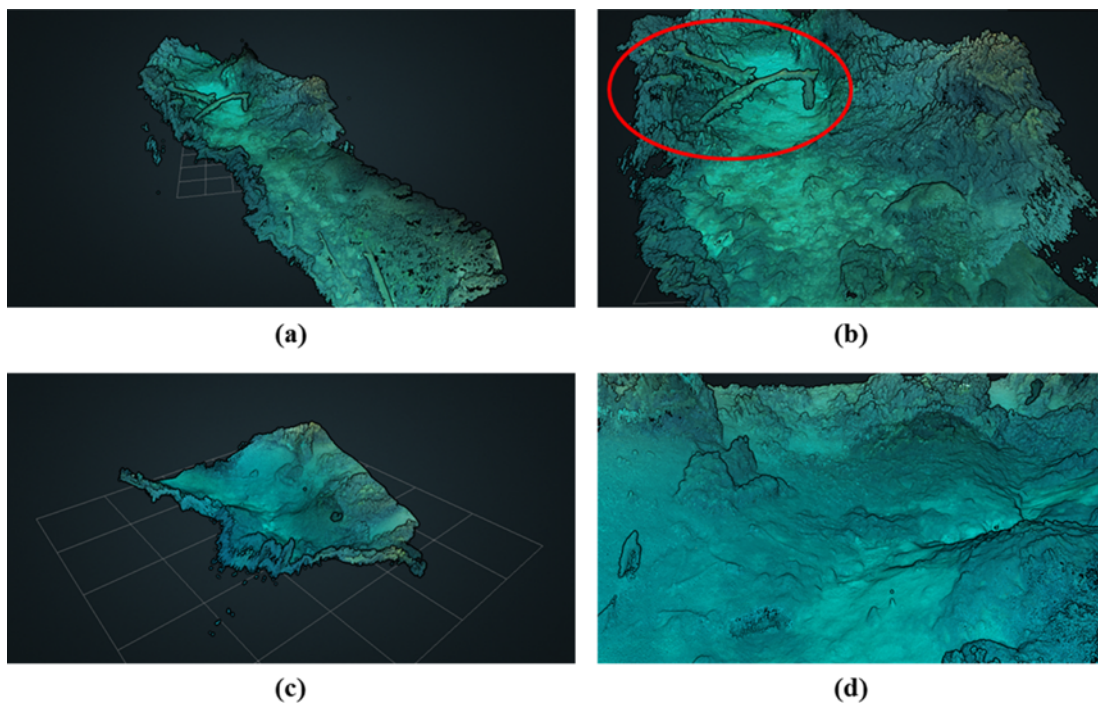


Fig. 6. The Display of the 3D Point Cloud on a Web Browser with Potree, which is a Web-based Point Cloud Viewer, of Study Site #1 and Site #2. Overall Area is Shown in (a) and (c), and (b) and (d) are Indicating Magnified Images.

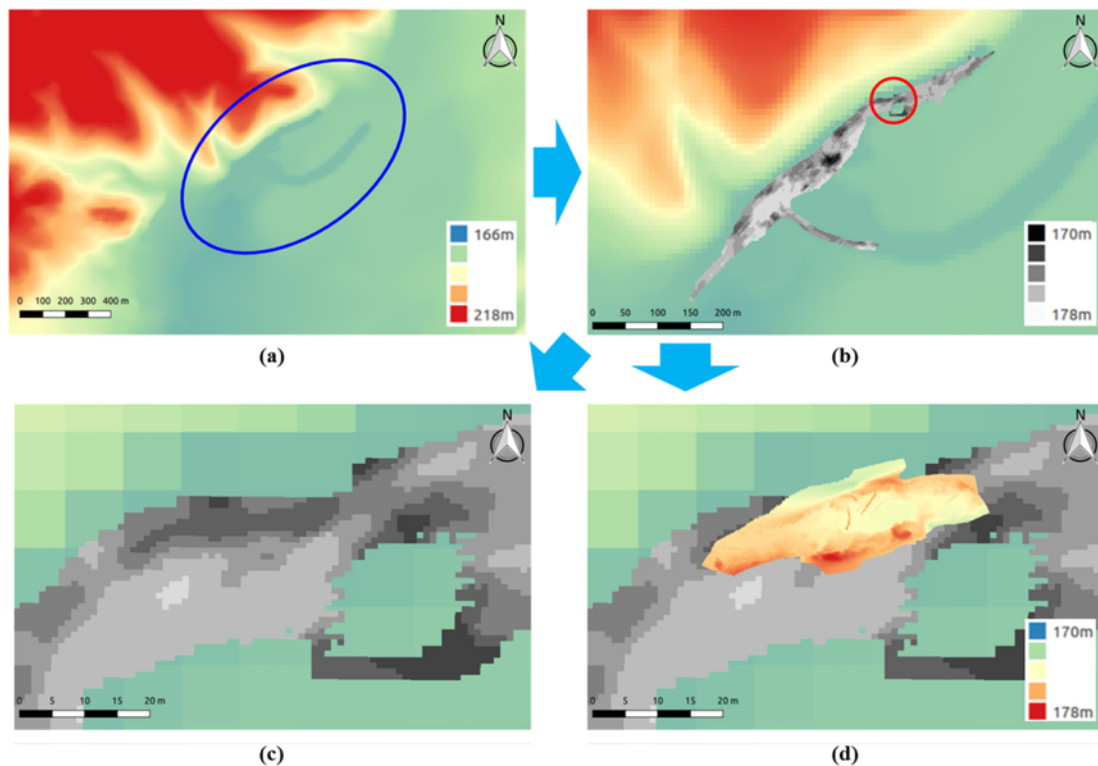


Fig. 7. The Display of the Bathymetric Maps from: (a) USGS DEM and (b) The SPS, (c) The Magnified Images of Study Site #1, (d) DSM Overlapped on the USGS DEM and Bathymetric Map from the SPS

displayed directly from 3D dense point cloud data including geo-coordinates and RGB color in this study. First of all, the point cloud was converted to HTML style with the Potree Converter

and displayed on a web browser (Fig. 6). Potree is unique in that it supports a very fast view and offers functions such as distance measurement for online service. The point cloud of test sites,

which consists of tens of millions of points, could be loaded within a few seconds in general internet browsers. Although the 3D point cloud of a partial area covered by weed and plants could not be generated because of the characteristics of SfM, the topographic surface of the lakebed was described in great detail. For instance, the branches located above the lakebed (red circle in Fig. 7(b)) and the fine parts of the lakebed (Fig. 7(d)) were generated with reasonable geometry. The 3D model of the test sites could be provided online for those interested in bathymetry, underwater surface investigation, or biogeographic signature analysis. Therefore, the proposed 3D mapping technique is feasible and useful for the researchers and other user groups in the GIS community.

4.3 Bathymetric Mapping

The DSM from the proposed method of study site #1 was compared with the two reference maps. The U.S. Geological Survey (USGS) is developing the 3D Elevation Program (3DEP) to serve high-quality topographic data (USGS). “1/3 arc-second”, which is the highest resolution seamless Digital Elevation Model (DEM) dataset for the United States, was used as a reference data, and spatial resolution is approximately 10 m. The latest version was published in 2013 for the study area. The bathymetric map generated by an acoustic Sub-bottom Profile System (SPS) was adopted as another reference data (Hooge *et al.*, 2016). The bathymetry survey was surveyed using “SB-424 sub-bottom profiling systems” (EdgeTech, Massachusetts, USA) in 2011 to map the lakebed. The frequency range of the SB-424 (4-24 kHz) was sufficient enough to penetrate the prevalent aquatic vegetation found on the lakebed and to obtain adequate imagery of the lake’s subsurface deposits if given sufficient depth in the water column. In extremely shallow area of the lake, acoustic voids occurred, and no data was acquired. Positioning of the SPS was acquired using DGPS to generate geo-referenced bathymetric map. The lakebed data was generated as contour data and converted to a grid map at a 1 m spatial resolution (Hooge *et al.*, 2016). The reference data and the results of the proposed method were converted to ASL elevation to compare simultaneously.

The bathymetric map from the SPS and DSM from the proposed method were overlapped over the DEM map from USGS (Fig. 7). Only few pixels indicate the lakebed of Spring Lake in the USGS DEM since the spatial resolution of DEM is about 10 m (Fig. 7(a)). It is not enough to be used as bathymetric map for ecological and archaeological applications. More detailed lake bed surface was generated by the SPS along surveying path. The advantage of the system’s generated bathymetric map is that it distinguishes between the vegetation layer and sediment on lake bottom with a penetrating acoustic signal (Fig. 7(b)). The proposed method generated a VHR bathymetric map having sub-centimeter spatial resolution although the coverage was smaller (Figs. 7(c) and 7(d)). The geo-referenced accuracy and detail of the VHR bathymetric map were validated as visually appropriate. In addition, the VHR bathymetric map could indicate

tiny objects such as branches in underwater.

The cross-section profiles were generated and compared to quantitatively evaluate the bathymetric map. Two profile lines were selected over the VHR bathymetric map as a cross shape (Fig. 8(a)). The elevation profiles of the USGS DEM (blue), SPS bathymetric map (red), and VHR bathymetric map (green) were drawn simultaneously in Figs. 8(b) and 8(c). The USGS DEM provided the flat lake bottom around 175 m as ASL. The elevation

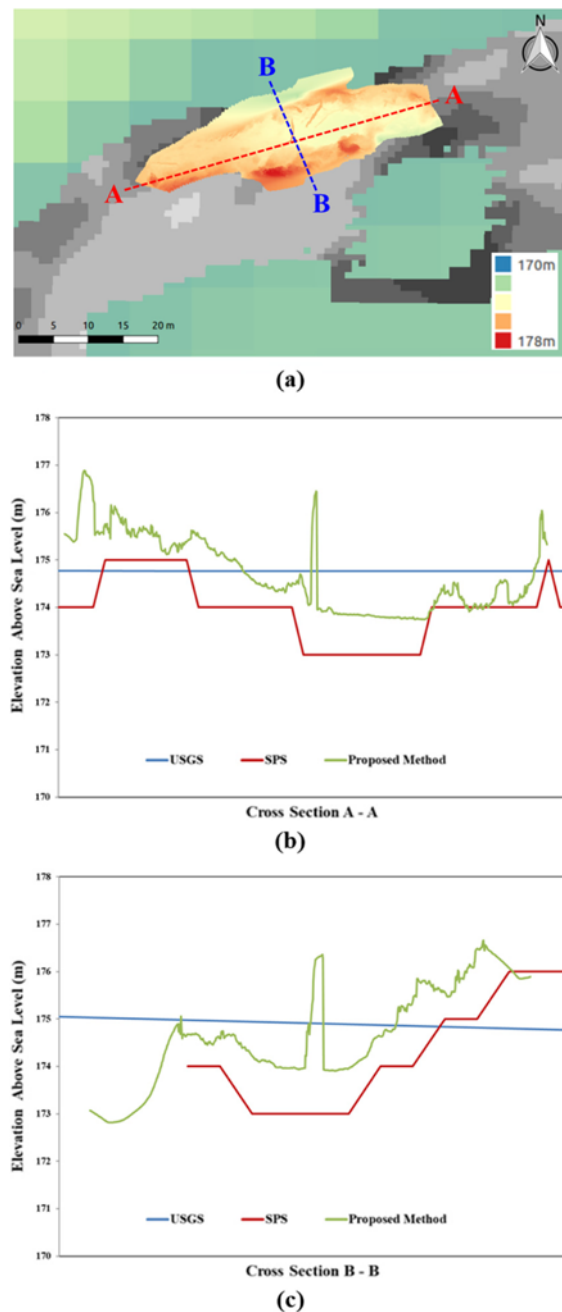


Fig. 8. Evaluation of the Bathymetric Maps: (a) Overlapped Bathymetric Maps with Two Cross-section Profile Lines (A-A and B-B). The Lengths of A-A and B-B are 46 m and 17 m, Respectively. The Bathymetric Profiles of (b) Cutting Line A-A, (c) Cutting Line B-B were Generated and Displayed Simultaneously.

Table 1. Correlation Coefficient (CC) and RMSE between Profiles of Bathymetric Maps from USGS, SPS, the Proposed Method

Cross section A-A				
Correlation coefficient (CC)		USGS	SPS	Proposed method
	USGS	1.00	0.32	0.68
	SPS	-	1.00	0.69
	Proposed method	-	-	1.00
RMSE (m)		USGS	SPS	Proposed method
	USGS	1.00	1.06	0.79
	SPS	-	1.00	0.96
	Proposed method	-	-	1.00
Cross section B-B				
Correlation coefficient (CC)		USGS	SPS	Proposed method
	USGS	1.00	-0.81	-0.74
	SPS	-	1.00	0.82
	Proposed method	-	-	1.00
RMSE (m)		USGS	SPS	Proposed method
	USGS	1.00	1.37	0.92
	SPS	-	1.00	1.10
	Proposed method	-	-	1.00

trend of profiles between the SPS and proposed method were very similar despite different sensor characteristics. Specifically, the elevation surface was perfectly matched in the cross-section profile B-B. In addition, the VHR bathymetric map represented a very finer surface of lakebed with higher precision while the SPS bathymetric map gave more detailed information like stepped shape than USGS DEM. For example, the peak of middle of the VHR bathymetric map indicates by a branch in Fig. 6(b).

We calculated the Correlation Coefficient (CC) and the Root Mean Square Error (RMSE) to figure out the difference between the DEM and bathymetric maps through the cross-section profiles because the bathymetric maps had different spatial resolution and coverage not overlapped perfectly (Table 1). It was meaningless to compare with USGS DEM since the surface was flat. However, the CC values between the SPS and the proposed method were larger than 0.7. There was a high correlation between the bathymetric maps from the SPS and the proposed method. The RMSE with SPS bathymetric map was calculated as about 1 m, which is affected by sensors' characteristic, GPS accuracy, GCP, and refraction. The main reason the gap occurred is the vegetation and sediment layer on the lakebed. Since the SPS is an active sensor, the signal for the system could penetrate the prevalent aquatic vegetation and measure the lake's sub-surface deposits. On the other hand, the proposed method adopted an optic camera to take hundreds of images with high overlap to generate a 3D point cloud of top surface of the lake bed including vegetation layer. Although GCPs can remove the error from GPS accuracy, refraction, and camera distortion, we processed the data without GCPs because of the stable conditions of the study area. However, refraction and camera calibration could cause a few centimeters of error (Dietrich, 2017; Harwin *et al.*, 2015). The error from no-GCPs processing

could be accepted for the aim of this study, which is rapid underwater mapping. In spite of several limitations, the proposed method can generate VHR bathymetric map.

5. Conclusions

In this study, a cost-effective and rapid method to generate 2D and 3D maps of underwater environments was successfully tested. We focused on the framework of data acquisition for 2D and 3D map construction with minimal human intervention. A digital camera with a waterproof housing (GoPro) and a cheap hand-held GPS logger were used to acquire raw underwater images and geo-location from the GPS signal. The location of the camera was determined by geo-tagging steps based on image acquisition time and GPS time. Agisoft Photoscan Pro software generated 3D point clouds and orthomosaic images from raw underwater images with partial EO for GPS logger. The color correction in $l\alpha\beta$ space was applied to the mosaic images for realistic 2D maps. A 3D map was generated from the 3D point clouds using Potree, which is an open source and web-based viewer for large scale point clouds. The results showed that detailed and realistic underwater maps were successfully obtained through this method. The VHR bathymetric map generated by the proposed method was compared with USGS DEM and the bathymetric map from the SPS. The CC and RMSE were calculated as 0.7 and 1 m, respectively. The results demonstrate that the proposed method could generate more detailed bathymetric map.

Although there are a few requirements such as clear water and calm surface conditions, it was verified that the proposed framework could provide faster and useful 2D/3D underwater maps to various users through an online service. The geo-tagging and color correction method adopted in this study could be applied to the various fields such as underwater survey, underwater ecology and underwater archaeology, among other fields. In the future, the IO and EO, which are affected by lens, waterproof housing and platform, will be measured to avoid the distortion of underwater mapping. A ROV system for underwater could be adopted for the proposed method to enhance data acquisition process with geo-location details. Accuracy evaluation of obtained 2D and 3D maps by the proposed method is the subject of future study.

References

- Atallah, L. and Probert Smith, P. J. (2003). "Using wavelet analysis to classify and segment sonar signals scattered from underwater sea beds." *International Journal of Remote Sensing*, RSPSoc, Vol. 24, No. 21, pp. 4113-4128, DOI: 10.1080/0143116021000035012.
- Balletti, C., Beltrame, C., Costa, E., Guerra, F., and Vernier, P. (2016). "3D reconstruction of marble shipwreck cargoes based on underwater multi-image photogrammetry." *Digital Applications in Archaeology and Cultural Heritage*, Vol. 3, No. 1, pp. 1-8, DOI: 10.1016/j.daach.2015.11.003.
- Balletti, C., Guerra, F., Tsioukas, V., and Vernier, P. (2014). "Calibration

- of action cameras for photogrammetric purposes.” *Sensors*, MDPI, Vol. 14, No. 9, pp. 17471-17490, DOI: 10.3390/s140917471.
- Bianco, G., Muzzupappa, M., Bruno, F., Garcia, R., and Neumann, L. (2015). “A new color correction method for underwater imaging.” *Proc. ISPRS XL-5/W5*, ISPRS, Piano di Sorrento, Italy, pp. 25-32, DOI: 10.5194/isprsarchives-XL-5-W5-25-2015.
- Brown, C. J. and Blondel, P. (2009). “Developments in the application of multibeam sonar backscatter for seafloor habitat mapping.” *Applied Acoustics*, Elsevier, Vol. 70, No. 10, pp. 1242-1247, DOI: 10.1016/j.apacoust.2008.08.004.
- Dietrich, J. T. (2017). “Bathymetric structure-from-motion: Extracting shallow stream bathymetry from multi-view stereo photogrammetry.” *Earth Surface Processes and Landforms*, Wiley, Vol. 42, No. 2, pp. 355-364, DOI: 10.1002/esp.4060.
- Ferrari, R., McKinnon, D., He, H., Smith, R. N., Corke, P., González-Rivero, M., Mumby, P. J., and Upcroft, B. (2016). “Quantifying multiscale habitat structural complexity: A cost-effective framework for underwater 3D modelling.” *Remote Sensing*, MDPI, Vol. 8, No. 2, pp. 113, DOI: 10.3390/rs8020113.
- Figueira, W., Renata, F., Weatherby, E., Porter, A., Hawes, S. and Byrne, M. (2015). “Accuracy and precision of habitat structural complexity metrics derived from underwater photogrammetry.” *Remote Sensing*, MDPI, Vol. 7, No. 12, pp. 16883-16900, DOI: 10.3390/rs71215859.
- Fonstad, M. A., Dietrich, J. T., Courville, B. C., Jensen, J. L., and Carbonneau, P. E. (2017). “Topographic structure from motion: A new development in photogrammetric measurement.” *Earth Surface Processes and Landforms*, Wiley, Vol. 38, No. 4, pp. 421-430, DOI: 10.1002/esp.3366.
- González-Rivero, M., Beijbom, O., Rodríguez-Ramírez, A., Holtrop, T., González-Marrero, Y., Ganase, A., Roelfsema, C., Phinn, S., and Hoegh-Guldberg, O. (2016). “Scaling up ecological measurements of coral reefs using semi-automated field image collection and analysis.” *Remote Sensing*, MDPI, Vol. 8, No. 1, p. 30, DOI: 10.3390/rs8010030.
- Google Street View (n.d.). <https://www.google.com/streetview/#oceans> [Accessed on Sept. 21, 2018].
- Harwin, S., Lucieer, A., and Osborn, J. (2015). “The impact of the calibration method on the accuracy of point clouds derived using unmanned aerial vehicle multi-view stereopsis.” *Remote Sensing*, MDPI, Vol. 7, No. 9, pp. 11933-11953, DOI: 10.3390/rs70911933.
- Hasan, R. C., Ierodiaconou, D., and Monk, J. (2012). “Evaluation of four supervised learning methods for benthic habitat mapping using backscatter from multi-beam sonar.” *Remote Sensing*, MDPI, Vol. 4, No. 11, pp. 3427-3443, DOI: 10.3390/rs4113427.
- Hooge, J., Hanselmann, F. H., Lohse, J. C., and Warren, D. (2016). *Spring lake underwater geoarchaeology survey*, The Meadow Center for Water and the Environment Center for Archaeological Studies, Texas State University, San Marcos, TX, USA.
- Johnson-Roberson, M., Pizarro, O., Williams, S. B., and Mahon, I. (2010). “Generation and visualization of large-scale three-dimensional reconstructions from underwater robotic surveys.” *Journal of Field Robot*, Wiley, Vol. 27, No. 1, pp. 21-51, DOI: 10.1002/rob.20324.
- Lowe, D. G. (2014). “Distinctive image features from scale-invariant keypoints.” *International Journal of Computer Vision*, Springer, Vol. 60, No. 2, pp. 91-110, DOI: 10.1023/B:VISI.0000029664.99615.94.
- Lu, D. and Cho, H. J. (2010). “An improved water-depth correction algorithm for seagrass mapping using hyperspectral data.” *Remote Sensing Letters*, RSPSoc, Vol. 2, No. 2, pp. 91-97, DOI: 10.1080/01431161.2010.502152.
- Reinhard, E., Ashikhmin, M., Gooch, B., and Shirley, P. (2001). “Color transfer between images.” *IEEE Computer Graphics and Applications*, IEEE, Vol. 21, No. 5, pp. 34-41, DOI: 10.1109/38.946629.
- Roberts, J. M., Brown, C. J., Long, D., and Bates, C. R. (2005). “Acoustic mapping using a multibeam echosounder reveals cold-water coral reefs and surrounding habitats.” *Coral Reefs*, Springer, Vol. 24, No. 4, pp. 654-669, DOI: 10.1007/s00338-005-0049-6.
- Roman, C. N., Inglis, G., Vaughn, J. I., Williams, S., Pizarro, O., Friedman, A., and Steinberg, D. (2011). “Development of high-resolution underwater mapping techniques.” *Oceanography*, The Oceanography Society, Vol. 24, No. 1, supplement, pp. 42-45, DOI: 10.5670/oceanog.24.1.supplement.
- Ruderman, D., Cronin, T., and Chiao, C. (1998). “Statistics of cone responses to natural images: Implications for visual coding.” *Journal of the Optical Society of America A*, OSA, Vol. 15, No. 8, pp. 2036-2045, DOI: 10.1364/JOSAA.15.002036.
- Schobesberger, D. and Patterson, T. (2008). “Evaluating the effectiveness of 2D vs. 3D trailhead maps.” *Proc. 6th ICA Mountain Cartography Workshop*, ICA, Lenk, Switzerland, pp. 201-205.
- Schuetz, M. (2016). *Potree: Rendering large point clouds in web browsers*, PhD Thesis, Vienna University of Technology, Wien, Austria.
- Shao, Z., Yang, N., Xiao, X., Zhang, L., and Peng, Z. (2016). “A multi-view dense point cloud generation algorithm based on low-altitude remote sensing images.” *Remote Sensing*, MDPI, Vol. 8, No. 5, pp. 381, DOI: 10.3390/rs8050381.
- Snavely, N., Seitz, S. M., and Szeliski, R. (2008). “Modeling the world from internet photo collections.” *International Journal of Computer Vision*, Springer, Vol. 80, No. 2, pp. 189-210, DOI: 10.1007/s11263-007-0107-3.
- USGS (n.d.). “The national map: 3D elevation program.” US Geological Survey, <https://www.usgs.gov/core-science-systems/ngp/3dep> [Accessed on Sept. 21, 2018].
- VanMiddlesworth, M., Kaess, M., Hover, F. S., and Leonard, J. J. (2015). “Mapping 3D underwater environments with smoothed submaps.” *Field and Service Robotics*, L. Mejjias, P. Corke, and J. Roberts, Ed., Springer, Cham, pp. 17-30, DOI: 10.1007/978-3-319-07488-7_2.
- Vierling, K. T., Vierling, L. A., Gould, W. A., Martinuzzi, S., and Clawges, R. M. (2008) “Lidar: Shedding new light on habitat characterization and modeling.” *Frontiers in Ecology and the Environment*, ESA, Vol. 6, No. 2, pp. 90-98, DOI: 10.1890/070001.
- Walker, B. K., Riegl, B., and Dodge, R. E. (2008). “Mapping coral reef habitats in Southeast Florida using a combined technique approach.” *Journal of Coastal Research*, CERF, Vol. 24, No. 5, pp. 1138-1150, DOI: 10.2112/06-0809.1.
- Wang, C. K. and Philpot, W. D. (2007). “Using airborne bathymetric lidar to detect bottom type variation in shallow waters.” *Remote Sensing of Environment*, Elsevier, Vol. 106, No. 1, pp. 123-135, DOI: 10.1016/j.rse.2006.08.003.
- Wolf, P. R. and DeWitte, B. A. (2000). *Elements of photogrammetry: With applications in GIS*, McGraw-Hill, New York, NY, USA.
- Zavalas, R., Ierodiaconou, D., Ryan, D., Rattray, A., and Monk, J. (2014). “Habitat classification of temperate marine macroalgal communities using bathymetric LiDAR.” *Remote Sensing*, MDPI, Vol. 6, No. 3, pp. 2154-5175, DOI: 10.3390/rs6032154.